

Spin waves in paramagnetic BCC iron: spin dynamics simulations

Xiuping Tao,¹ D. P. Landau,¹ T. C. Schulthess,² and G. M. Stocks³

¹Center for Simulation Physics, University of Georgia, Athens, GA 30602

²Computer Science and Mathematics Division, Oak Ridge National Laboratory, Oak Ridge, TN 37831-6164

³Metals and Ceramics Division, Oak Ridge National Laboratory, Oak Ridge, TN 37831-6114

(Dated: March 22, 2024)

Large scale computer simulations are used to elucidate a longstanding controversy regarding the existence, or otherwise, of spin waves in paramagnetic BCC iron. Spin dynamics simulations of the dynamic structure factor of a Heisenberg model of Fe with first principles interactions reveal that well defined peaks persist far above Curie temperature T_c . At large wave vectors these peaks can be ascribed to propagating spin waves, at small wave vectors the peaks correspond to over-damped spin waves. Paradoxically, spin wave excitations exist despite only limited magnetic short-range order at and above T_c .

PACS numbers: 75.10.Hk, 75.40.-s, 75.40.Gb, 75.50.Bb

Keywords: transition metal, spin dynamics, Heisenberg model, short-range order

For over three decades, the nature of magnetic excitations in ferromagnetic materials above the Curie temperature T_c has been a matter of controversy amongst experimentalists and theorists alike. Early neutron scattering experiments on iron suggested that spin waves were renormalized to zero at T_c [1]; however, in 1975, using unpolarized neutron scattering techniques, Lynn at Oak Ridge (ORNL) reported [2] that spin waves in iron persisted as excitations up to the highest temperature measured ($1.4T_c$), and no further renormalization of the dispersion relation was observed above T_c .

Experimentally, it was challenged primarily by Shirane and collaborators at Brookhaven (BNL) [3]. Using polarized neutrons, they reported that spin wave modes were not present above T_c and suggested that the ORNL group needed polarized neutrons to subtract the background scattering properly. Utilizing full polarization analysis techniques the ORNL group subsequently confirmed their earlier work and, in addition, they analyzed data from both groups and concluded that their resolution was more than an order of magnitude better than that employed by the BNL researchers [4]. Moreover, angle-resolved photoemission studies [5, 6] suggested the existence of magnetic short-range order (SRO) in paramagnetic iron and that this could give rise to propagating modes. Theoretically, SRO of rather long length scales (25 \AA) was postulated to exist far above T_c [7, 8] and a more subtle kind was proposed later [9]. Contrarily, it was also suggested that above T_c , all thermal excitations are dissipative [10, 11]. To further complicate matters, analytical calculations for a Heisenberg model of iron, with exchange interactions extending to fifth-nearest neighbors and a three pole approximation [12], did not reproduce the line shape measured by either experimental group mentioned above. In addition, Shastry [13] performed spin dynamics (SD) simulations of a nearest neighbor Heisenberg model of paramagnetic iron with 8192 spins and showed some plots of dynamic structure factor $S(\mathbf{q}; \omega)$ with a shoulder at nonzero ω for some \mathbf{q} . It was explained to be due to statistical errors instead of

propagating modes.

With new algorithmic and computational capabilities, qualitatively more accurate SD simulations can now be performed. In particular, it can follow many more spins for much longer integration time. We use these techniques and a model designed specifically to emulate BCC iron and have been able to unequivocally identify propagating spin wave modes in the paramagnetic state, lending substantial support to Lynn's [2] experimental findings. Interestingly, spin waves are found despite only limited magnetic SRO.

To describe the high temperature dynamics we use a classical Heisenberg model $H = \sum_{\mathbf{r} \in \mathbf{r}^0} \sum_{\mathbf{r}' \in \mathbf{r}^0} J_{\mathbf{r}\mathbf{r}'} S_{\mathbf{r}} \cdot S_{\mathbf{r}'}$, for which the exchange interactions, $J_{\mathbf{r}\mathbf{r}'}$, are obtained from first principles electronic structure calculations. For Fe this is a reasonable approximation since the size of the magnetic moments associated with individual Fe-sites are only weakly dependent on the magnetic state [14] and by including interactions up to fourth nearest neighbors it is possible to obtain a reasonably good T_c .

Large scale computer simulations using SD techniques to study the dynamic properties of Heisenberg ferromagnets [15] and antiferromagnets [16] have been quite effective, and the direct comparison of RbMnF_3 SD simulations with experiments was especially satisfying [16]. We have adopted these techniques and used $L_x = L_y = L_z$ BCC lattices with periodic boundary conditions and $L = 32$ and 40 . At each lattice site, there is a three-dimensional classical spin of unit length (we absorb spin moments into the definition of the interaction parameters) and each spin has a total of 50 interacting neighbors. We use interaction parameters, J_i , for the $T = 0$ ferromagnetic state of BCC Fe calculated using the standard formulation [17] and the layer-KKR method [18]. The calculated values are $J_1 = 36.3386 \text{ meV}$, $J_2 = 20.6520 \text{ meV}$, $J_3 = 1.625962 \text{ meV}$, and $J_4 = 2.39650 \text{ meV}$.

In our simulations, a hybrid Monte Carlo method was used to study the static properties and to generate equilibrium configurations as initial states for integrating the coupled equations of motion of SD [19]. At T_c and for

$L = 32$, the measured nonlinear relaxation time in the equilibrating process and the linear relaxation time between equilibrated states for the total energy and for the magnetization [20] are both smaller than 500 hybrid steps per spin. We discarded 5000 hybrid steps (for equilibration) and used every 5000th hybrid step's state as an initial state for the SD simulations. For the J_i 's used here, $T_c = 919(1)\text{K}$, which is slightly smaller than the experimental value $T_c^{\text{exp}} = 1043\text{K}$. The equilibrium magnetization $j_{\text{eq}} = (1/N) \sum_r S_r^z$ ($T = T_c$)¹⁼³ in the vicinity of T_c and this is in agreement with experiments.

The SD equations of motion are

$$\frac{dS_r}{dt} = H_{\text{eff}} S_r; \quad (1)$$

where $H_{\text{eff}} = J_{r,r^0} S_{r^0}$ is an effective field at site r due to its interacting neighbors. The integration of the equations determines the time dependence of each spin and was carried out using an algorithm based on second-order Suzuki-Trotter decompositions of exponential operators as described in [21]. The algorithm views each spin as undergoing Larmor precession around its effective field H_{eff} , which is itself changing with time. To deal with the fact that we are considering four shells of interacting neighbors, the BCC lattice is decomposed into sixteen sublattices. This algorithm allows time steps as large as $\tau = 0.05$ (in units of $\tau_0 = J_1^{-1}$). Typically, the integration was carried out to $t_{\text{max}} = 20000 \tau = 1000\tau_0$.

The space- and time-displaced spin-spin correlation function $C^k(r - r^0; \tau)$ and the related dynamical structure factor, $S^k(q; \omega)$, are fundamental in the study of spin dynamics [22] and are defined as

$$C^k(r - r^0; \tau) = \langle S_r^k(\tau) S_{r^0}^k(0) \rangle - \langle S_r^k(\tau) \rangle \langle S_{r^0}^k(0) \rangle; \quad (2)$$

where $k = x, y$ or z and the angle brackets $\langle \dots \rangle$ denote the ensemble average, and

$$S^k(q; \omega) = \sum_{r, r^0} \int_0^{2\pi} e^{iq \cdot (r - r^0)} \int_0^{2\pi} e^{i\omega \tau} C^k(r - r^0; \tau) \frac{d\tau}{2}; \quad (3)$$

where q and ω are momentum and energy (E / \hbar) transfer respectively. It is $S^k(q; \omega)$ that was probed in the neutron scattering experiments discussed earlier.

By calculating partial spin sums 'on the fly' [15], it is possible to calculate $S^k(q; \omega)$ without storing a huge amount of data associated with each spin configuration. Because L is finite, only a finite set of q values are accessible: $q = 2\pi n_q / (La)$ with $n_q = 1; 2; \dots; L$ for the $(q; 0; 0)$ and $(q; q; q)$ directions and $n_q = 1; 2; \dots; L/2$ for the $(q; q; 0)$ direction. (a is lattice constant.) For $T = T_c$, the ensemble average in Eq. 2 was performed using at least 2000 starting configurations. We average $S^k(q; \omega)$ over equivalent directions and this averaged structure factor is denoted as $S(q; \omega)$.

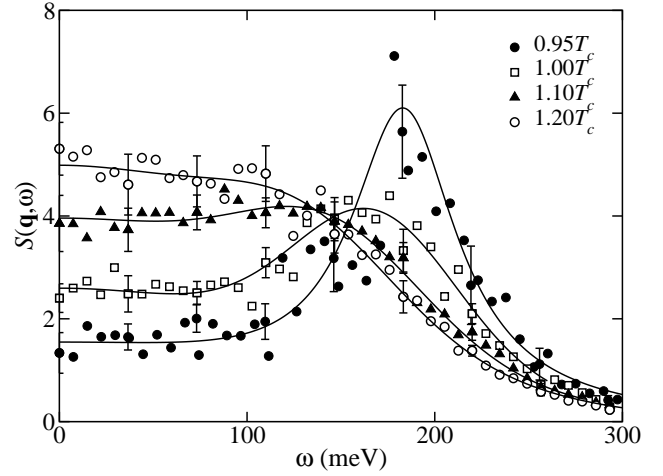


FIG. 1: Calculated energy dependence of $S(q; \omega)$ at $q = \pi a(1; 0; 0)$ and for $T = 0.95T_c$ (700 runs), $1.0T_c$ (2000 runs), $1.1T_c$ (2240 runs), and $1.2T_c$ (2240 runs) for $L = 32$. The solid lines are fits to the data as explained in text. Error bars are shown at a few typical points.

In Fig. 1 we show the frequency dependence of $S(q; \omega)$ obtained for four different temperatures around T_c . These, so called, constant- q scans are for $q = \pi a(1; 0; 0)$ ($\Delta j = 1.09 \text{ \AA}^{-1}$), which is half way to Brillouin Zone boundary. At $0.95T_c$, $S(q; \omega)$ already has a 3-peak structure: one weak central peak at zero energy and two symmetric spin wave peaks (we only show data for $\omega \geq 0$ since the structure factor is symmetric about $\omega = 0$). Note that the spin wave peaks are already quite wide. As T goes to T_c and above, the central peak becomes more pronounced. In addition, the spin wave peaks shift to lower energies, broaden further and become less obvious, however they still persist. This 3-peak structure at high temperatures is in contrast to the 2-peak spin wave structure found at low temperatures. In the neutron scattering from $^{54}\text{Fe}(12\% \text{ Si})$ experiments [4], Mook and Lynn also noticed a central peak, but could not decide whether it was intrinsic to pure iron or a result of alloying of silicon.

In general, constant- q scans are isotropic in the $(q; 0; 0)$, $(q; q; 0)$, and $(q; q; q)$ directions. For very small Δj there is only a central peak in the scans (as is expected) and the 3-peak structure only develops for larger Δj . We fit the 3 peaks in $S(q; \omega)$ using different fitting functions and found the best results with either a Gaussian central peak plus two Lorentzian peaks at ω_0 :

$$S(q; \omega) = G + L_+ + L_-; \quad (4)$$

or a Gaussian central peak plus two additional Gaussian peaks at ω_0 :

$$S(q; \omega) = G + G_+ + G_-; \quad (5)$$

where $G = I_c \exp(-\omega^2 / \omega_c^2)$, $L_{\pm} = I_0 \omega_1^2 / ((\omega - \omega_0)^2 + \omega_1^2)$, and $G_{\pm} = I_0 \exp(-(\omega - \omega_0)^2 / \omega_1^2)$. For moderate Δj the results are fit best with Eq. 4, while Eq. 5 works better

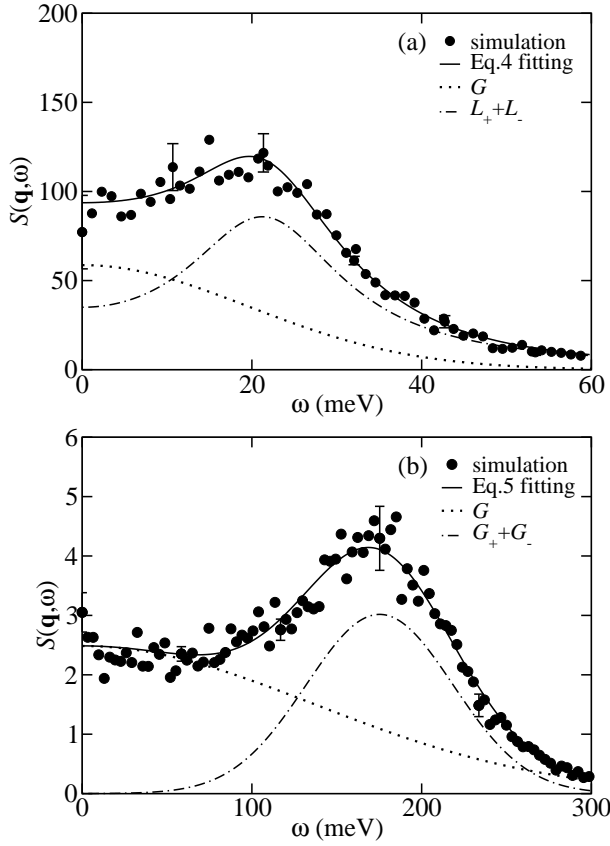


FIG. 2: Fits to $S(\mathbf{q}; \omega)$ at $T = T_c$ for two q_j points along the $(q_j; q_j; 0)$ direction for $L = 32$. (a) $q_j = 0.48 \text{ \AA}^{-1}$ fit to Eq. 4, with $I_c = 58.7$, $J_c = 27.6 \text{ meV}$, $I_0 = 80.6$, $J_0 = 21.4 \text{ meV}$, and $J_1 = 11.3 \text{ meV}$; (b) $q_j = 1.16 \text{ \AA}^{-1}$ fit to Eq. 5 with $I_c = 2.49$, $J_c = 193.3 \text{ meV}$, $I_0 = 3.02$, $J_0 = 175.3 \text{ meV}$, and $J_1 = 61.2 \text{ meV}$. The vertical scale in (b) is much smaller than that in (a). Error bars are shown at a few typical points.

at larger q_j . In Fig. 2 we show, for $T = T_c$, the results of fitting constant- q scans at $q_j = 0.48 \text{ \AA}^{-1}$ and $q_j = 1.16 \text{ \AA}^{-1}$ in the $(q_j; q_j; 0)$ direction. The $q_j = 0.48 \text{ \AA}^{-1}$ result fits well to Eq. 4 and has $J_1 = J_0 < 1$, i.e., the excitation lifetime is longer than its period and thus it can be regarded as a spin wave excitation. It should be noted that this q_j value is very close to that (0.47 \AA^{-1}) for which Lynn found propagating modes in contradiction to the findings of the BNL group. At $q_j = 1.16 \text{ \AA}^{-1}$, the structure factor has much weaker intensity and fits best to Eq. 5 with a ratio $J_1 = J_0$ that is even smaller than at $q_j = 0.48 \text{ \AA}^{-1}$. This is illustrative of the general conclusion that the propagating nature of the excitation modes is most pronounced at large q_j .

Figure 3 shows the dispersion relations obtained by plotting the peak positions, ω_0 , determined from the fits to $S(\mathbf{q}; \omega)$ along the $(q_j; q_j; 0)$ direction. Calculated dispersion curves are shown at several temperatures in the ferromagnetic and paramagnetic phases together with the ex-

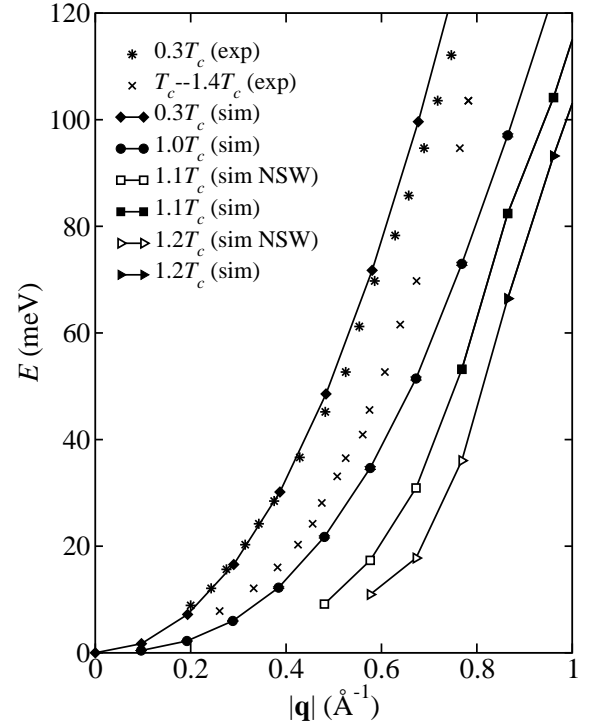


FIG. 3: Comparison of dispersion curves obtained in our simulations (sim) with Lynn's experimental (exp) (Ref. [2]) results for the $(q_j; q_j; 0)$ direction. Open symbols indicate excitations with mixed nature and are not due to spin waves (NSW).

perimental results of Lynn [2]. To estimate errors, we fitted each constant- q scan several times by cutting off the tail at slightly different ω_{max} to get an average ω_0 ; these error bars are found to be no larger than symbols. In this figure, filled symbols indicate modes that are clearly propagating ($J_1 = J_0 < 1$) while open symbols indicate that, even though there are peaks at $\omega_0 \neq 0$, the peaks have widths $J_1 > J_0$. The calculated result for $T = 0.3T_c$ is very close to that from the experiments and propagating modes exist for very small q_j . For $T = T_c$, our curves lie below the experiments' and soften with increasing temperatures, a property not seen in the experiments. One possibility deserving of further study is that our use of temperature and configuration independent exchange interactions, in particular those appropriate to the $T = 0$ ferromagnetic state, breaks down at high temperatures when the spin moments are highly non-collinear.

In our simulations we have equal access to constant- q scans and constant- E scans; however, this is not the case in neutron scattering experiments. Because the dispersion curves of Fe are generally very steep, experimentalists usually perform constant- E scans. In Fig. 4 we show constant- E scans for several E values at $T = 1.1T_c$ based on simulations. Clearly, the constant- E scans have two peaks (symmetric about $q_j = 0$) that become smaller and wider and shift to higher q_j as E increases. Peaks in constant- E

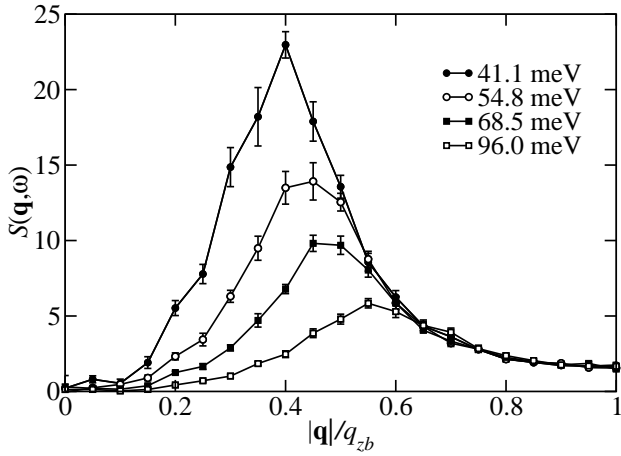


FIG. 4: $T = 1.1T_c$ constant-E scans along $(q; q; 0)$ direction for $E = 41.1$ meV, 54.8 meV, 68.5 meV, and 96.0 meV with $L = 40$. Brillouin Zone boundary $q_{zb} = 1.55 \text{ \AA}^{-1}$ in the direction.

scans strongly suggest that SRO persists above T_c [7].

The degree of magnetic SRO can be obtained directly from the behavior of static correlation function $C^k(r; r^0; 0)$ (i.e. Eq. 2 with $t = 0$), which can be calculated from the Monte Carlo configurations alone. For $T = 1.1T_c$ we find a correlation length of approximately $2a$ (6 neighbor shells), indicative of only limited SRO. Thus, in general, extensive SRO is not required to support spin waves. Moreover, inspection of Fig. 3 for $T = 1.1T_c$ shows that the point $q \approx 0.77 \text{ \AA}^{-1}$, at which these peaks first correspond to propagating modes, is when their wavelength ($\approx 2a$) first becomes the order of the static correlation length.

In summary, our SD simulations clearly point to the existence of spin waves in the paramagnetic state of BCC Fe and support the original conclusions of Lynn. Their signature is seen as spin wave peaks in dynamical structure factor in constant- q and constant-E scans. Detailed analysis of the constant- q scans shows that the propagating nature of these excitations is clearest at large q in agreement with experiment. This is also consistent with the requirement that their wavelength be the order of, or shorter than, the static correlation length. While the inclusion of four shells of first-principles-determined interactions into the Heisenberg model makes our results specifically relate to BCC Fe, we have also found spin waves in a Heisenberg model containing only nearest neighbor interactions. In addition to elucidating the longstanding controversy regarding the existence of spin waves above T_c , these simulations also point to the important role that inelastic neutron scattering studies of the paramagnetic state can have in understanding the nature of magnetic excitations, particularly when coupled with state-of-the-art SD simulations.

We thank Shan-Ho Tsai, H. K. Lee, V. P. Antropov, and

K. Binder for informative discussions. Computations were performed at ORNL-CCS (www.ccs.ornl.gov) and NERSC (www.nersc.gov) using elements of the *-Mag* toolset which may be obtained at <http://mri-fre.ornl.gov/psimag>. Work supported by Computational Materials Science Network sponsored by DOE BES-DMSE (XT), BES-DMSE (GMS), NSF Grant No. DMR-0341874 (XT and DPL) and DARPA (XT and TCS) under contract No. DE-AC05-00OR22725 with UT-Battelle LLC.

Electronic address: txp@uga.edu

- [1] M. F. Collins, V. J. Minkiewicz, R. Nathans, L. Passell, and G. Shirane, Phys. Rev. **179**, 417 (1969).
- [2] J. W. Lynn, Phys. Rev. B **11**, 2624 (1975).
- [3] J. P. Wicksted, G. Shirane, and O. Steinsvoll, Phys. Rev. B **29**, R488 (1984); G. Shirane, O. Steinsvoll, Y. J. Uemura, and J. Wicksted, J. Appl. Phys. **55**, 1887 (1984); J. P. Wicksted, P. Boni, and G. Shirane, Phys. Rev. B **30**, 3655 (1984).
- [4] H. A. Mook and J. W. Lynn, J. Appl. Phys. **57**, 3006 (1985).
- [5] E. M. Haines, V. Heine, and A. Ziegler, J. Phys. F: Metal Phys. **15**, 661 (1985); E. M. Haines, R. Clauberg, and R. Feder, Phys. Rev. Lett. **54**, 932 (1985).
- [6] E. Kisker, R. Clauberg, and W. Gudat, Z. Phys. B **61**, 453 (1985).
- [7] V. Korenman, J. L. Murray, and R. E. Prange, Phys. Rev. B **16**, 4032 (1977); R. E. Prange and V. Korenman, Phys. Rev. B **19**, 4691 (1978).
- [8] H. Capellmann, Solid State Commun. **30**, 7 (1979); Z. Phys. B **35**, 269 (1979).
- [9] V. Heine and R. Joynt, Europhys. Lett. **5**, 81 (1988).
- [10] J. Hubbard, Phys. Rev. B **20**, 4584 (1979); Phys. Rev. B **23**, 5974 (1981).
- [11] T. Moriya, J. Magn. Magn. Mat. **100**, 261 (1991).
- [12] B. S. Shastry, D. M. Edwards, and A. P. Young, J. Phys. C **14**, L665 (1981).
- [13] B. S. Shastry, Phys. Rev. Lett. **53**, 1104 (1984).
- [14] A. J. Pindor, J. Staunton, G. M. Stocks, and H. Winter, J. Phys. F **13**, 979 (1983).
- [15] K. Chen and D. P. Landau, Phys. Rev. B **49**, 3266 (1994).
- [16] S.-H. Tsai, A. Bunker, and D. P. Landau, Phys. Rev. B **61**, 333 (2000).
- [17] A. I. Liechenstein, M. I. Katsnelson, V. P. Antropov, and V. A. Gubanov, J. Mag. Mag. Mater. **67**, 65 (1987).
- [18] T. C. Schulthess and W. H. Butler, J. App. Phys. **83**, 7225 (1998).
- [19] P. Peczak and D. P. Landau, Phys. Rev. B **47**, 14260 (1993).
- [20] D. P. Landau and K. Binder, *A Guide to Monte Carlo Simulations in Statistical Physics* (Cambridge University Press, Cambridge, 2000).
- [21] M. Krech, A. Bunker, and D. P. Landau, Comput. Phys. Commun. **111**, 1 (1998).
- [22] S. W. Lovesey, *Theory of neutron scattering from condensed matter* (Clarendon, Oxford, 1984).